Charging Behavior of Single-Stranded DNA Polyelectrolyte Brushes

Gang Shen,[†] Napoleon Tercero,[†] Mariafrancis A. Gaspar,[†] Bindhu Varughese,[‡] Kenneth Shepard,[§] and Rastislav Levicky*[†,||]

Contribution from the Department Chemical Engineering, Columbia University, New York, New York 10027, Department Chemistry and Biochemistry XPS Facility, University of Maryland, College Park, Maryland 20742, and Department Electrical Engineering, Columbia University, New York, New York 10027

Received October 20, 2005; E-mail: rlevicky@poly.edu

Abstract: DNA monolayers are widely used in fundamental and applied genomics and are versatile experimental models for elucidating the behavior of charged polymers at interfaces. The physical behavior of these systems is to a large extent governed by their internal ionic microenvironment, which is investigated here for layers of end-tethered, single-stranded DNA oligonucleotides (DNA brushes). Retention of counterions by the DNA brush manifests as lowered susceptibility of the interfacial capacitance to external salt conditions. A physical model based on concepts adapted from polymer science was used to further elucidate the connection between monolayer organization and its charging behavior. The data indicate a reorganization of the monolayer with changes in ionic strength and strand coverage that is consistent with that expected for a polyelectrolyte brush. A method for electrochemical quantification of strand coverage, based on shift of reduction potential for redox counterions associated with the DNA monolayer, is also described. These results provide guidance for development of label-free electrochemical diagnostics employing DNA monolayers and formulate a description of monolayer behavior within a polymer science framework.

Introduction

Monolayers of immobilized nucleic acids are central to a portfolio of technologies for applied genomics, including sequencing by synthesis,[1,2] genotyping and polymorphism identification,[3,4] gene expression profiling,[5] and biosensing.[6-9] They are also promising experimental models for investigating fundamental properties of charged polymers at solid−liquid interfaces.[10] These applications share a common interest in understanding how nucleic acid monolayers organize and how their organization influences activity toward hybridization or other biomolecular interactions. An important research direction has been to establish structure−function relationships, for example, by correlating monolayer density with hybridization activity[11-19] or with duplex melting transitions.[20-22]

Events of interest, such as hybridization or enzymatic sequencing, must take place under conditions existing within the monolayer. In general the local ionic strength and composition vary greatly from the bulk solution, and there is ample evidence that these differences exert pronounced influence over thermodynamics and kinetics of processes involving surface-tethered DNA chains.[23] A better understanding of the local conditions is therefore critical to more effective use of DNA films in diagnostic and other applications.

[†] Department Chemical Engineering, Columbia University.
[‡] University of Maryland.
[§] Department Electrical Engineering, Columbia University.
[||] Current address: Department Chemical and Biological Engineering, Polytechnic University, Brooklyn, NY 11201.

(1) Braslavsky, I.; Hebert, B.; Kartalov, E.; Quake, S. R. *Proc. Natl. Acad. Sci. U.S.A.* **2003**, *100*, 3960−3964.
(2) Seo, T. S.; Bai, X. P.; Kim, D. H.; Meng, Q. L.; Shi, S. D.; Ruparel, H.; Li, Z. M.; Turro, N. J.; Ju, J. Y. *Proc. Natl. Acad. Sci. U.S.A.* **2005**, *102*, 5926−5931.
(3) Nikiforov, T. T.; Rendle, R. B.; Goelet, P.; Rogers, Y.-H.; Kotewicz, M. L.; Anderson, S.; Trainor, G. L.; Knapp, M. R. *Nucleic Acids Res.* **1994**, *22*, 4167−4175.
(4) Matsuzaki, H. et al. *Genome Res.* **2004**, *14*, 414−425.
(5) Schena, M.; Shalon, D.; Davis, R. W.; Brown, P. O. *Science* **1995**, *270*, 467−470.
(6) Gooding, J. J. *Electroanalysis* **2002**, *14*, 1149−1156.
(7) Drummond, T. G.; Hill, M. G.; Barton, J. K. *Nat. Biotechnol.* **2003**, *21*, 1192−1199.
(8) Brockman, J. M.; Nelson, B. P.; Corn, R. M. *Annu. Rev. Phys. Chem.* **2000**, *51*, 41−63.
(9) Wang, J. *Anal. Chim. Acta* **2002**, *469*, 63−71.
(10) Johnson, P. A.; Gaspar, M. A.; Levicky, R. *J. Am. Chem. Soc.* **2004**, *126*, 9910−9911.
(11) Peterson, A. W.; Heaton, R. J.; Georgiadis, R. M. *Nucleic Acids Res.* **2001**, *29*, 5163−5168.
(12) Pena, S. R. N.; Raina, S.; Goodrich, G. P.; Fedoroff, N. V.; Keating, C. D. *J. Am. Chem. Soc.* **2002**, *124*, 7314−7323.
(13) Stevens, P. W.; Henry, M. R.; Kelso, D. M. *Nucleic Acids. Res.* **1999**, *27*, 1719−1727.
(14) Herne, T. M.; Tarlov, M. J. *J. Am. Chem. Soc.* **1997**, *119*, 8916−8920.
(15) Chan, V.; Graves, D. J.; McKenzie, S. E. *Biophys. J.* **1995**, *69*, 2243−2255.
(16) Vainrub, A.; Pettitt, B. M. *Phys. Rev. E* **2002**, *66*, 041905.
(17) Erickson, D.; Dongqing, L.; Krull, U. J. *Anal. Biochem.* **2003**, *317*, 186−200.
(18) Hagan, M. F.; Chakraborty, A. K. *J. Chem. Phys.* **2004**, *120*, 4958−4968.
(19) Halperin, A.; Buhot, A.; Zhulina, E. B. *Clin. Chem.* **2004**, *50*, 2254−2262.
(20) Peterlinz, K. A.; Georgiadis, R. M.; Herne, T. M.; Tarlov, M. J. *J. Am. Chem. Soc.* **1997**, *119*, 3401−3402.
(21) Watterson, J. H.; Piunno, P. A. E.; Wust, C. C.; Krull, U. J. *Langmuir* **2000**, *16*, 4984−4992.
(22) Meunier-Prest, R.; Raveau, S.; Finot, E.; Legay, G.; Cherkaoui-Malki, M.; Latruffe, N. *Nucleic Acids. Res.* **2003**, *31*, e150.
(23) Levicky, R.; Horgan, A. *Trends Biotechnol.* **2005**, *23*, 143−149.

In this study, electrochemical methods are used to probe the internal environment in monolayers of single-stranded DNA (ssDNA) chains as a function of bulk ionic strength and chain surface coverage. The strands are immobilized by one end to a solid support, in a "polyelectrolyte brush" geometry.[24] The charging, or capacitive, response is determined, and a physical framework is formulated to relate experimental observations to monolayer organization. The principal conclusions can be explained by existence of high ionic strength inside the DNA monolayer even at low concentrations of bulk salt and by the "softness" of the monolayer structure, that is, the response of the structure to variations in salt concentration and chain coverage. A method for electrochemical quantification of immobilized strand surface density, based on the electrochemical work needed to reduce redox-active counterions trapped in the DNA monolayer, is also described.

Materials and Methods

Details of experimental procedures and data analysis are provided in the Supporting Information. All electrochemical measurements used a Ag/AgCl/3 M NaCl reference electrode, and all quoted potentials are relative to this reference. A Pt wire served as the counter electrode, and a 3 mm diameter polycrystalline Au disk electrode, as the working electrode. The working electrode was etched electrochemically to achieve a reproducible initial state, and its roughness factor r (r = true area/geometric area; $r \geq 1$) was measured from the double layer capacitance.[25] r ranged from 2.56 to 3.25 (average 2.87 ± 0.28). Single-stranded, oligothymine Thy_{25}–S–S–$(CH_2)_3OH$ chains were immobilized onto the working electrode from 1 μM solutions in 1 M $MgCl_2$. $MgCl_2$ facilitates achievement of high coverages.[26,27] The attachment was via the disulfide-modified 3′ terminus. After immobilization of the Thy_{25} strands, the electrodes were exposed to 1 mM mercaptopropanol (MCP) in 18.2 MΩ cm water for 1 h to passivate the remnant electrode surface and to block nonspecific interactions between the strands and the support. MCP is expected to form a hydrophilic, hydroxyl-terminated monolayer that resists nonspecific adsorption of ssDNA.[14,28] An all Thy sequence was used because, of the four bases, thymine exhibits the weakest affinity for gold[29–31] making this sequence optimal for realizing an end-tethered brush geometry.

Differential capacitance per area, C_d, was measured as a function of Thy_{25} surface coverage (0 to 2.1 × 10^{13} cm^{-2}) and bulk ionic strength (0.008 M to 1 M NaCl or KCl) using electrochemical impedance spectroscopy (EIS). EIS measurements were carried out under non-faradaic conditions at 0 V dc bias, 5 mV ac amplitude, and frequencies from 10 Hz to 100 000 Hz. Reported C_d values have been corrected for surface roughness by scaling the geometric electrode area by r.

Following EIS characterization, cyclic voltammetry (CV) traces were obtained at 0.08 V/s in background electrolyte of 10 mM tris-(hydroxymethyl)amino methane (tris base), pH 7.4, with and without 1 μM hexaamineruthenium(III) chloride (RuHex). The peak potential V_{peak} for reduction of monolayer-associated $RuHex^{3+}$, $RuHex^{3+}$-(monolayer) + e^- → $RuHex^{2+}$(monolayer), was determined by fitting a quadratic polynomial to identify the peak maximum after subtraction

of charging currents. $RuHex^{3+}$ acts as a counterion to the negative charge on the DNA strands. V_{peak} was correlated with coverage of Thy_{25} strands which was determined independently with X-ray photoelectron spectroscopy (XPS), using working electrodes prepared on glass slides. XPS was performed on a Kratos Axis 165 instrument with a hemispherical analyzer and Mg Kα source, 225 W X-ray power, 80 eV pass energy, and 90° (normal to sample) takeoff angle. A wide pass energy was used to improve signal intensity at the expense of energy resolution. DNA coverages were calculated from P 2p intensities following the procedure of Petrovykh et al.[32]

Results and Discussion

Determination of ssDNA Coverage from the Reduction Potential of $RuHex^{3+}$ Counterions. Interaction of redox-active counterions with DNA is well-known to alter thermodynamics of their redox processes, whether the DNA is in solution[33,34] or present as surface-immobilized species.[35–39] Here we consider the dependence of such effects on the coverage of ssDNA chains in the relatively crowded environment of a monolayer, for Thy_{25} ssDNA molecules and the redox counterion $RuHex^{3+}$. As is the case for $RuHex^{3+}$ interacting with double-stranded DNA,[40–42] its interaction with ssDNA is similarly expected to be predominantly electrostatic.

Figure 1A shows measured CV curves for the reaction $RuHex^{3+}$(monolayer) + e^- → $RuHex^{2+}$(monolayer) for three different Thy_{25} coverages. As coverage increases, the reduction peak potential V_{peak} systematically shifts toward more negative values, indicating that the $RuHex^{3+}$ state is stabilized relative to $RuHex^{2+}$ with increasing DNA coverage. Origins of this stabilization are discussed below. As expected for surface adsorbed redox species,[43] the peak currents were observed to increase linearly with scan rate. Because of the low 1 μM concentration of $RuHex^{3+}$ in bulk solution, only reduction of $RuHex^{3+}$ cations trapped in the DNA monolayer is clearly seen on the cathodic scan. A close examination of the peak envelopes reveals, nevertheless, broadening toward more positive potentials. The broadening is predominantly attributed to concurrent reduction of solution $RuHex^{3+}$, which occurs close to −0.15 V. This is more clearly seen in the inset to Figure 1A where, at a higher 27 μM $RuHex^{3+}$ concentration, reduction of both surface and solution species can be discerned. Such bimodal waves were earlier observed for $RuHex^{3+}$ and DNA films by Tarlov and co-workers.[44,45]

Returning to the main panel of Figure 1A, the peaks narrow at higher strand coverages, with the width (fwhm) decreasing

(24) Miklavic, S. J.; Marcelja, S. *J. Phys. Chem.* **1988**, *92*, 6718–6722.
(25) Oesch, U.; Janata, J. *Electrochim. Acta* **1983**, *28*, 1237–1246.
(26) Petrovykh, D. Y.; Kimura-Suda, H.; Whitman, L. J.; Tarlov, M. J. *J. Am. Chem. Soc.* **2003**, *125*, 5219–5226.
(27) Kelley, S. O.; Barton, J. K.; Jackson, N. M.; McPherson, L. D.; Potter, A. B.; Spain, E. M.; Allen, M. J.; Hill, M. G. *Langmuir* **1998**, *14*, 6781–6784.
(28) Levicky, R.; Herne, T. M.; Tarlov, M. J.; Satija, S. K. *J. Am. Chem. Soc.* **1998**, *120*, 9787–9792.
(29) Kimura-Suda, H.; Petrovykh, D. Y.; Tarlov, M. J.; Whitman, L. J. *J. Am. Chem. Soc.* **2003**, *125*, 9014–9015.
(30) Storhoff, J. J.; Elghanian, R.; Mirkin, C. A.; Letsinger, R. L. *Langmuir* **2002**, *18*, 6666–6670.
(31) Wolf, L. K.; Gao, Y.; Georgiadis, R. M. *Langmuir* **2004**, *20*, 3357–3361.

(32) Petrovykh, D. Y.; Kimura-Suda, H.; Tarlov, M. J.; Whitman, L. J. *Langmuir* **2004**, *20*, 429–440.
(33) Carter, M. T.; Rodriguez, M.; Bard, A. J. *J. Am. Chem. Soc.* **1989**, *111*, 8901–8911.
(34) Welch, T. W.; Corbett, A. H.; Thorp, H. H. *J. Phys. Chem.* **1995**, *99*, 11757–11763.
(35) Millan, K. M.; Mikkelsen, S. R. *Anal. Chem.* **1993**, *65*, 2317–2323.
(36) Kelley, S. O.; Barton, J. K.; Jackson, N. M.; Hill, M. G. *Bioconjugate Chem.* **1997**, *8*, 31–37.
(37) Pang, D. W.; Abruna, H. D. *Anal. Chem.* **1998**, *70*, 3162–3169.
(38) Tani, A.; Thomson, A. J.; Butt, J. N. *Analyst* **2001**, *126*, 1756–1759.
(39) Yang, W.; Ozsoz, M.; Hibbert, D. B.; Gooding, J. J. *Electroanalysis* **2002**, *14*, 1299–1302.
(40) Ho, P. S.; Frederick, C. A.; Saal, D.; Wang, A. H. J.; Rich, A. *J. Biomol. Struct. Dyn.* **1987**, *4*, 521–534.
(41) Karthe, P.; Gautham, N. *Acta Crystallogr., Sect. D* **1998**, *D54*, 501–509.
(42) Boon, E. M.; Jackson, N. M.; Wightman, M. D.; Kelley, S. O.; Hill, M. G.; Barton, J. K. *J. Phys. Chem. B* **2003**, *107*, 11805–11812.
(43) Laviron, E. *J. Electroanal. Chem.* **1974**, *52*, 355–393.
(44) Steel, A. B.; Herne, T. M.; Tarlov, M. J. *Anal. Chem.* **1998**, *70*, 4670–4677.
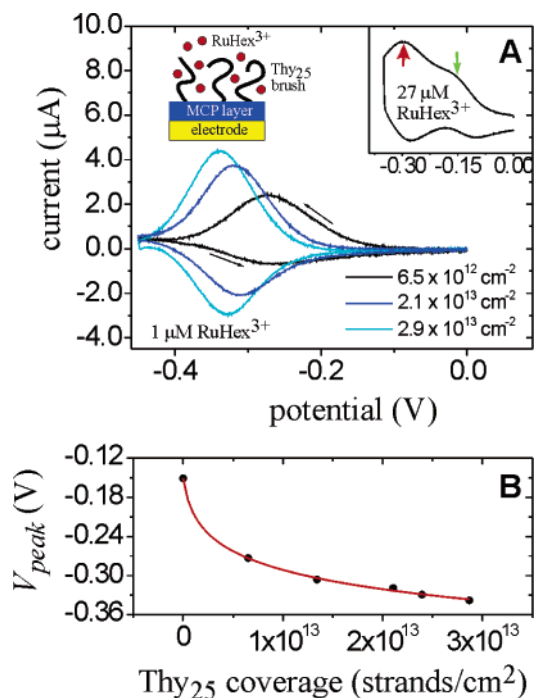(45) Steel, A. B.; Herne, T. M.; Tarlov, M. J. *Bioconjugate Chem.* **1999**, *10*, 419–423.

Figure 1. Effect of Thy$_{25}$ coverage on the peak potential (V_{peak}) for the reduction of brush-associated RuHex^{3+} counterions. All potentials are relative to a Ag/AgCl/3 M NaCl reference. (A) CV traces at three strand coverages. Charging currents have been subtracted. Conditions: 1 μM RuHex^{3+}, 10 mM tris, pH 7.4, scan rate 0.08 V/s. *Inset graph*: Data at higher, 27 μM concentration of RuHex^{3+}, showing contributions from monolayer-associated RuHex^{3+} (thick red arrow) as well as solution RuHex^{3+} (thin green arrow). Thy$_{25}$ coverage was 1.2×10^{13} cm^{-2}. Also shown is a schematic depiction of the monolayer structure. (B) V_{peak} as a function of Thy$_{25}$ coverage determined independently with XPS. The solid line is a two-parameter interpolation (see text), with $P_1 = 9.8 \times 10^{-22}$ cm^2 mol/L and $P_2 = 1.64$ ($R^2 = 0.999$).

from 125 mV for the coverage of 6.5×10^{12} cm^{-2} to 100 mV for the 2.9×10^{13} cm^{-2} sample. This narrowing with increasing chain coverage presumably results from the greater relative magnitude of the surface reduction current. However, even the highest coverages do not reach the theoretical width of 90 mV expected for a reversible reaction of noninteracting, surface-confined species.[46] In this regard, it is worth noting that broadened peak envelopes are expected even when there is no convolution of surface and solution signals, on the grounds that not all brush-confined RuHex^{3+} cations can be assumed to experience an identical local environment. The potential difference between cathodic and anodic peaks for brush-associated RuHex is found to be 8 mV, close to the 0 mV expected for reversibly behaving surface species. However, it is significant that the RuHex cations are not strictly immobilized. Indeed, the reverse scans exhibit decreased current magnitudes, an effect attributed to a lowered affinity of RuHex^{2+} for the DNA compared to RuHex^{3+}. A lowered electrostatic affinity of RuHex^{2+} for DNA is expected to facilitate its displacement from the brush by other cations (i.e., tris$^+$), as reflected in the decreased current magnitudes on the reverse scan. Figure 1B plots the reduction potential V_{peak} as a function of strand coverage that was determined independently using XPS. A systematic correlation between V_{peak} and strand coverage is evident.

Why does the RuHex^{3+} reduction potential shift with strand coverage? Experimental[47−50] and theoretical[51−53] reports have identified a variety of contributions to shifts in redox potentials of surface-confined species compared to solution values, including changes in the local dielectric constant, spatial distribution, solvation, coverage, ion pair formation, and image charge interactions. Many of these effects may also apply in the present case, although their clear separation is challenged by the complexity of the DNA brush environment. Nevertheless, a dominant contribution lies in the coupling of the reduction of RuHex^{3+} to the transport of cations from solution. When RuHex^{3+} inside the DNA brush is reduced, a local deficit of positive charge is created. The deficit triggers an inflow of additional cations in order to preserve electroneutrality of the near-surface region that contains the immobilized, negative DNA charge. If the cation transport occurs up a gradient in activity, then work must be performed to "pump" the cations into the monolayer, corresponding to a negative displacement in V_{peak}. In general, the activity of cations in the DNA brush will be higher than in solution because of accumulation by the monolayer. Moreover, this difference should be enhanced at higher chain coverages, leading to a greater displacement of V_{peak}. Similar effects have been reported with thiol monolayers of small molecules[54,55] and with membrane coatings,[56] where the induced potentials are often referred to as Donnan potentials.

In the present experiments, tris$^+$ was by far the most abundant cation in solution, and its transport is expected to dominate. This expectation is confirmed in Figure 2 by noting that changing RuHex^{3+} solution concentration does not significantly alter V_{peak}, whereas lowering tris$^+$ concentration further shifts the wave in the negative direction. Boon et al. have reported a similar ionic strength dependence for monolayers of double-stranded DNA.[42] A shift in V_{peak} with a decrease in tris$^+$ ionic strength will also in part derive from an increased resistance of the electrolyte, due to a higher potential drop across the solution. However, even at the lowest (1 mM) concentration of tris, contributions from such uncompensated resistance were found to be only 4 mV, a small fraction of the experimentally observed displacements.

From stoichiometry, it is expected that reduction of a single RuHex^{3+} requires transport of a single tris$^+$ cation. The resultant electrochemical work, if performed reversibly, is $eN_A\Delta V = RT \ln(a_{tris}/A_{tris})$, where e is the negative electronic charge, N_A is Avogadro's number, ΔV is the potential shift, R is the gas constant, T is absolute temperature, and a_{tris} and A_{tris} are activities of tris$^+$ in the monolayer and in solution, respectively. If the displacement in V_{peak} is solely attributed to tris transport into the monolayer, then for the experimental conditions

(46) Laviron, E. *J. Electroanal. Chem.* **1979**, *101*, 19−28.

(47) Rowe, G. K.; Creager, S. E. *Langmuir* **1991**, *7*, 2307−2312.
(48) Creager, S. E.; Rowe, G. K. *J. Electroanal. Chem.* **1997**, *420*, 291−299.
(49) Avecedo, D.; Abruna, H. D. *J. Phys. Chem.* **1991**, *95*, 9590−9594.
(50) De Long, H. C.; Buttry, D. A. *Langmuir* **1992**, *8*, 2491−2496.
(51) Smith, C. P.; White, H. S. *Anal. Chem.* **1992**, *64*, 2398−2405.
(52) Ohtani, M.; Kuwabata, S.; Yoneyama, H. *Anal. Chem.* **1997**, *69*, 1045−1053.
(53) Andreu, R.; Calvente, J. J.; Fawcett, W. R.; Molero, M. *Langmuir* **1997**, *13*, 5189−5196.
(54) Redepenning, J.; Tunison, H. M.; Finklea, H. O. *Langmuir* **1993**, *9*, 1404−1407.
(55) Bretz, R. L.; Abruna, H. D. *J. Electroanal. Chem.* **1996**, *408*, 199−211.
(56) Doblhofer, K.; Armstrong, R. D. *Electrochim. Acta* **1988**, *33*, 453−460.
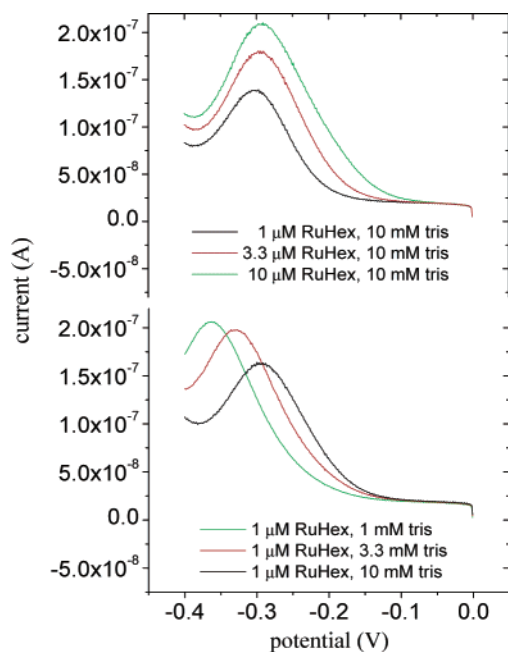
Figure 2. Voltammograms for reduction of brush-associated RuHex^{3+}. (Top) At three concentrations of RuHex^{3+} in 10 mM tris. (Bottom) At three concentrations of tris and 1 μM RuHex^{3+}. Other conditions: pH 7.4, scan rate 0.08 V/s, chain coverage 1.2×10^{13} cm^{-2}.

$$V_{\text{peak}}(\sigma_{\text{DNA}}) = -0.151 - 0.026 \ln(a_{\text{tris}}/\Phi_{\text{tris}}) \qquad (1)$$

The value -0.151 V is the measured reduction potential at zero DNA coverage, and the solution activity of tris$^+$ was approximated by its molar concentration Φ_{tris}.[57]

Application of eq 1 to predict V_{peak} would require information on the dependence of a_{tris} on the strand coverage σ_{DNA}, which is not known. Trials of simple functional forms revealed good agreement for a power law dependence, $a_{\text{tris}} = \Phi_{\text{tris}} + P_1\sigma_{\text{DNA}}{}^{P_2}$, as shown by the solid line in Figure 1B. The resultant fit can be used to estimate what values of a_{tris} are required to account for the observed shifts in V_{peak}. Following this reasoning, a_{tris} is estimated to range from about 1 (σ_{DNA} of 6.4×10^{12} cm^{-2}) to about 10 (σ_{DNA} of 2.6×10^{13} cm^{-2}), with a strong dependence on σ_{DNA} given by an exponent of $P_2 = 1.64$.

The large estimated values for a_{tris} at high chain coverage are revealing. Typical values of counterion activity coefficients in polyelectrolyte solutions are often found to be around 0.5, or even lower.[58] If similarly low activity coefficients apply to a DNA brush, then the surface concentration of tris$^+$ under high chain coverage must be significantly greater than 10 M, an unlikely scenario. Thus, despite the success of eq 1 as an interpolation formula in Figure 1B, it seems evident that work associated with tris$^+$ transport only partially accounts for the observed V_{peak} shifts. For example, if higher chain coverages more strongly favor formation of DNA−RuHex^{3+} contacts relative to DNA−RuHex^{2+} contacts, that preference would also manifest as an additional contribution to V_{peak}. Such effects are being assessed in a separate study.

Compared to other nondestructive electrochemical methods for measuring chain coverage, such as those based on total charge required to reduce redox counterions associated with a DNA film,[44,59] the present approach is particularly straightforward as it only requires knowledge of V_{peak}. Integration of peak
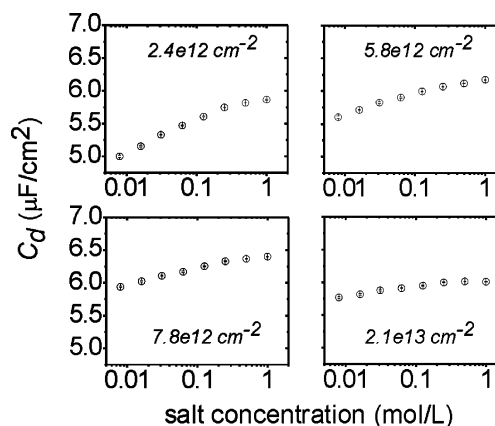
Figure 3. ssDNA monolayer capacitance C_d as a function of monovalent salt concentration, at different strand coverages. All graphs are on common y- and x-scales. Conditions: pH 7.0 solution of NaCl in water, 5 mV rms ac amplitude, 0 V dc vs Ag/AgCl/3 M NaCl. Coverages were determined from the peak potential V_{peak} using the RuHex method, Figure 1B. Error bars (horizontal lines across symbols) indicate the standard deviation of two measurements taken 4 min apart.

areas, which are subject to uncertainties in quantitatively separating out background currents,[51] is avoided. Moreover, by adjusting the solution ionic strength, the sensitivity of V_{peak} to chain coverage can be tuned, with greater displacements for a given coverage realized at lower ionic strengths (Figure 2 bottom).

Charging Behavior of ssDNA Monolayers. Measurements of interfacial capacitance provide a direct probe of the near surface conditions, and as such are especially useful for exploring how the local conditions relate to those in solution. Figure 3 shows the differential capacitance C_d (capacitance/ area) for ssDNA monolayers immersed in aqueous solutions containing only NaCl as the electrolyte. C_d is plotted as a function of increasing salt from 8 mM to 1 M and four strand coverages from 2.4×10^{12} to 2.1×10^{13} cm^{-2}. For all coverages, C_d increases with ionic strength, qualitatively consistent with the behavior of a diffuse double layer at a bare solid−liquid interface.[60] Interestingly, however, the sensitivity of C_d to salt concentration diminishes at higher strand coverages, with a progressive flattening of the C_d vs salt concentration curves. Also evident in Figure 3 are vertical offsets, manifested as a translation along the y-axis, between C_d curves for different coverages; these offsets are attributed to uncertainty in the determination of the roughness r used for area normalization of the capacitance.

The weakening dependence of C_d on solution salt at higher strand coverages is a signature that conditions within the monolayer increasingly deviate from those in solution. Intuitively, one important reason for this should be that the DNA brush retains its counterions, maintaining a high local ionic strength even if little or no salt is present in the bulk electrolyte. If C_d reflects this decoupling between local and bulk ionic strength, its change with variations in bulk salt should be suppressed, as observed experimentally.

(57) The concentration of the tris cation is governed by the tris pK_a, which is 8.3 at ambient temperature. Thus, at a pH of 7.4 and tris concentration of 10 mM, the concentration of the tris$^+$ cation is 8.9 mM.
(58) Rice, S. A.; Nagasawa, M. *Polyelectrolyte Solutions*; Academic Press: New York, 1961.
(59) Yu, H.-Z.; Luo, C.-Y.; Sankar, C. G.; Sen, D. *Anal. Chem.* **2003**, *75*, 3902−3907.
(60) Bard, A. J.; Faulkner, L. R. *Electrochemical Methods: Fundamentals and Applications*, 2nd ed.; Wiley & Sons: New York, 2000.
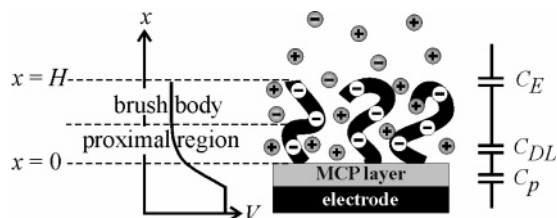
Figure 4. Model used in the derivation of the charging response of a polyelectrolyte brush. The expected potential profile is schematically indicated on the left, and the equivalent circuit description is shown on the right.

The connection between the charging response, as captured in C_d, and the structure of the DNA layer can be further explored using a simple model. The model assumes that the DNA charges are immobile and uniformly distributed throughout the layer; that is, the DNA concentration profile is approximated by a step function of thickness H (Figure 4). Notably, treatment of the DNA charge as immobile neglects perturbations of the chain configurations due to the 5 mV potential modulation used to measure C_d. Thus, the model attributes the ac charging currents during measurement of C_d entirely to the movement of small (Na^+, Cl^-) ions. These mobile ions pass freely between the layer and the external electrolyte, the external electrolyte occupying the space $x > H$ (Figure 4). Inside the brush, the DNA chains provide a background of constant negative charge density. In addition, the presence of net charge on the working electrode produces an electric field that interacts with salt ions in the "proximal region" (Figure 4), altering their spatial distribution. The surface field decays with distance such that, in the main brush body, it can be taken as zero. This division of the brush into two sections, a proximal and a brush body region, is valid only if the electrostatic screening (Debye) length r_D within the DNA layer is sufficiently less than the layer thickness H, i.e., $r_D/H \ll 1$. For the experimental conditions (Supporting Information), r_D/H is expected to remain below 0.2, and typically be closer to 0.1. Thus, surface fields are expected to decay sufficiently rapidly for the two-region description of the brush, as illustrated in Figure 4, to be reasonable.

Within the above description, three putative contributions to the overall capacitance C_d can be identified (Figure 4): (i) capacitance of the MCP layer (C_p), (ii) a diffuse layer capacitance inside the DNA layer, at the MCP−brush interface (C_{DL}), and (iii) capacitance associated with the brush−solution interface (C_E), where a charge separation arises due to partial "leakage" of brush counterions beyond the physical confines of the brush.[61] The charge separation associated with C_E reflects a balance between entropy favoring expansion of the counterion cloud and electrostatic interactions favoring its containment within the DNA film.

The EIS experiments measure differential capacitance $C_d = dq/dV$, where dq is a differential change in charge density stored by the brush in response to an increment dV in potential applied across it. Because the brush−solution interface is permeable to salt it follows that, in a measurement of differential capacitance, C_E is effectively short-circuited and does not contribute. The expression for C_d thus simplifies to a series arrangement of C_p and C_{DL},

$$C_d = C_p C_{DL}/(C_p + C_{DL}) \tag{2}$$

C_p is assumed constant as determined by the thickness and dielectric constant of the MCP layer. In contrast, the diffuse

layer capacitance C_{DL} must reflect conditions in the solvated interior of the DNA film. This capacitance is analogous to the classical Gouy−Chapman model[60] in that it is associated with a diffuse distribution of ions but differs in that the diffuse ionic atmosphere exists inside the charge background provided by the DNA. The expression for C_{DL}, assuming a uniform distribution of immobile DNA charge, is derived analytically from Poisson's equation in the Supporting Information. The result is

$$C_{DL} = \mp \left(\frac{eN_A \epsilon \epsilon_0}{2}\right)^{1/2}$$
$$\frac{c_+(1 - e^{-eV_0/kT}) + c_-(e^{eV_0/kT} - 1)}{\left[(c_+ - c_-)V_0 + \frac{kTc_-}{e}(e^{eV_0/kT} - 1) + \frac{kTc_+}{e}(e^{-eV_0/kT} - 1)\right]^{1/2}} \tag{3}$$

where c_i is concentration of monovalent salt ions of charge i in the brush body, V_0 is the potential at $x = 0$ relative to bulk electrolyte, ϵ is the dielectric constant, ϵ_0 is the permittivity of vacuum, and k is the Boltzmann constant. The "−" sign applies for $V_0 < 0$, and the "+" sign, for $V_0 > 0$. The concentrations of anions (c_-) and cations (c_+) in the body of the brush can be related to their concentrations $\Phi_+ = \Phi_- = \Phi$ in the external electrolyte by the constraints of local charge neutrality and partitioning equilibrium (Donnan equilibria),[62,63]

$$c_{DNA} + c_- = c_+ \text{(charge neutrality)} \tag{4}$$

$$c_+/\Phi_+ = \Phi_-/c_- \text{(Donnan equilibria)} \tag{5}$$

In eq 5, ionic activities have been approximated by concentrations. The assumption of charge neutrality in the brush body is supported by recent simulations of strongly charged brushes[64] as well as by results from earlier lattice theory calculations.[65] Equations 4 and 5 are readily solved for c_- and c_+ in terms of Φ and c_{DNA},

$$c_+ = \frac{c_{DNA}}{2} + \left(\frac{c_{DNA}^2}{4} + \Phi^2\right)^{1/2} \qquad c_- = \Phi^2/c_+ \tag{6}$$

The concentration of immobilized charge attributed to the DNA, c_{DNA}, is given by $c_{DNA} = Q\sigma_{DNA}/N_A H$, where Q is the number of charges per strand. Since only those positive ions that are freely mobile (i.e., uncondensed on the DNA backbone[66,67]) are expected to participate in the charging response, in eq 3 c_+ is taken to represent the concentration of uncondensed cations. Consistency then requires that, in $c_{DNA} = Q\sigma_{DNA}/N_A H$, the parameter Q is the reduced charge per strand, accounting for counterion condensation. For ssDNA, Q is about 60% of the total phosphate charge.[67] Based on theoretical predictions for polyelectrolyte brushes,[61,68] H is taken to follow a scaling law in chain coverage and salt concentration, $H = K\sigma_{DNA}^w \Phi^{-v}$, with w and v as the scaling exponents. Equations 2, 3, and 6 describe

(61) Borisov, O. V.; Zhulina, E. B.; Birshtein, T. M. *Macromolecules* **1994**, *27*, 4795−4803.
(62) Donnan, F. G. *J. Membrane Sci.* **1995**, *100*, 45−55.
(63) Zhulina, E. B.; Borisov, O. V.; Birshtein, T. M. *Macromolecules* **1999**, *32*, 8189−8196.
(64) Kumar, N. A.; Seidel, C. *Macromolecules* **2005**, *38*, 9341−9350.
(65) Israels, R.; Leermakers, F. A. M.; Fleer, G. J.; Zhulina, E. B. *Macromolecules* **1994**, *27*, 3249−3261.
(66) Manning, G. S. *Acc. Chem. Res.* **1979**, *12*, 443−449.
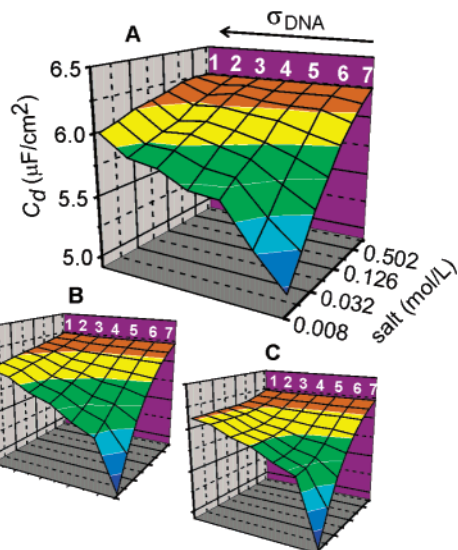(67) Record, M. T.; Anderson, C. F.; Lohman, T. M. *Quart. Rev. Biophys.* **1978**, *11*, 103−178.

Figure 5. Comparison of experimental and calculated C_d values as a function of salt concentration and strand coverage. All plots are on common *xyz* scale, shown in (A). Strand coverages are indicated by numbers along the top of plot (A) in order of decreasing coverage: (1) 2.1×10^{13} cm^{-2}, (2) 1.5×10^{13} cm^{-2}, (3) 7.8×10^{12} cm^{-2}, (4) 5.8×10^{12} cm^{-2}, (5) 3.4×10^{12} cm^{-2}, (6) 2.4×10^{12} cm^{-2}, (7) pure MCP monolayer. (A) Experimental data. (B) C_d response for the RM model. $w = 0.0 \pm 0.17$, $v = 0.28 \pm 0.05$, $C_p = 6.38 (\pm 0.03) \times 10^{-6}$ F/cm^2, $V_0 = -0.017 (\pm 0.006)$ V. Uncertainties reflect 10% increase in rms error. Fixed parameters: $\epsilon = 78$, $\epsilon_0 = 8.85 \times 10^{-12}$ C^2 N^{-1} m^{-2}, $e = 1.60 \times 10^{-19}$ C, $N_A = 6.02 \times 10^{23}$ mol^{-1}, $T = 298$ K, $k = 1.38 \times 10^{-23}$ J/K. (C) C_d response for the SM model. $H = 10$ nm, $C_p = 6.38 \times 10^{-6}$ F/cm^2, $V_0 = -0.017$ V. For purposes of comparison, the curve for each coverage in (A) was rescaled by a constant factor (between 0.97 and 1.06) so as to equalize C_d at 1 M with that measured for the pure MCP sample. This adjustment lies within experimental uncertainty of the roughness factor r used for area normalization of the capacitance.

the predicted behavior of C_d for a polyelectrolyte brush as a function of strand coverage and salt concentration.

Figure 5 compares experimental C_d data (Figure 5A) to predicted trends for two scenarios differing in assumptions regarding behavior of the DNA brush. In the "responsive" monolayer (RM) scenario, Figure 5B, the brush swells or shrinks with changes in salt and strand coverage according to the scaling law expression for H, $H = K\sigma_{DNA}{}^w\Phi^{-v}$. C_p, V_0, w, and v were varied to optimize agreement between calculated and experimental C_d, subject to the constraint that H not exceed the total contour length of the chains. K was calculated from v and w and published neutron reflectivity data on a 25mer ssDNA brush[28] which found $H = 4.8$ nm when $\sigma_{DNA} = 3 \times 10^{12}$ cm^{-2} and $\Phi = 1$ M.[69] In the second, "stiff" monolayer (SM) scenario, Figure 5C, H was fixed at 10 nm.

The RM model approximately reproduces experimental trends over the investigated range in σ_{DNA} and Φ, exhibiting a gradual decrease in capacitance with a decrease in ionic strength. The optimized exponent values $w = 0.0 \pm 0.17$ and $v = 0.28 \pm 0.05$ can be compared to those predicted for highly charged polyelectrolyte brushes,[68] in particular for the so-called saturated osmotic ($w = v = 0$) and quasineutral ($w = \frac{1}{3}$, $v = \frac{1}{3}$) regimes spanned by our experimental conditions.[70] The fit is seen to be rather insensitive to w, as evident from the large uncertainty, presumably because the experimental range in σ_{DNA} was modest. The value for v falls between the saturated osmotic and

quasineutral predictions, as may be expected since the measurements straddle these regimes. However, the comparison to theory should not be overemphasized since the theory applies in the limit of long chains, compared to the rather short Thy$_{25}$ molecules, and since the brush thickness H was not measured directly but rather was deduced through a model-dependent calculation of C_d under simplifying assumptions. For the SM case (Figure 5C), C_d asymptotes to a constant value at the lowest salt concentrations, contrary to the experimental trend. In the SM scenario, as bulk ionic strength decreases, the ion concentration in the brush (and hence C_d) converges to a constant value because the brush thickness H is fixed. In contrast, in the RM description the monolayer swells as Φ decreases, causing a dilution of the internal ion concentration that manifests as a progressive, gradual decrease in C_d. The essential point is that responsive behavior is expected on physical grounds[61,68] and, as argued by the comparison of experimental data with the RM and SM scenarios, is also reflected in the charging response of a DNA polyelectrolyte brush.

Conclusions

Electrochemical techniques were used to probe the ionic microenvironment inside of monolayers of end-attached ssDNA oligonucleotides (DNA brushes). The reduction potential of redox counterions associated with the monolayer progressively shifts toward negative potentials with increasing chain coverage. This effect is partially an outcome of electrical work needed to bring additional counterions into the monolayer, against a concentration gradient, to preserve its electroneutrality. Calibration of the shift against an independent measure of chain surface coverage leads to a simple and robust method for quantifying amounts of immobilized ssDNA. The capacitance of ssDNA monolayers was studied as a function of bulk salt concentration and strand coverage. Retention of counterions by the monolayers manifested as a decreased susceptibility of the capacitance to the external salt environment. Moreover, the charging response exhibited signatures of structural reorganization whereby the DNA strands stretch or relax with changes in solution ionic strength, consistent with expected physical behavior of charged polymer layers. These results emphasize that the ionic environment inside a DNA brush differs strikingly from that in solution and are relevant to DNA bioassays[71−74] and related technologies based on monitoring of interfacial electrostatics in nucleic acid films.

(68) O'Shaughnessy, B.; Yang, Q. *arXiv:cond-mat/0408036* **2005**, art. no. 0408036.

(69) For an ssDNA monolayer of uniform internal composition, of thickness H, the z-rms thickness defined in ref 28 is equal to $H/12^{1/2}$.

(70) The transition between the two regimes has been observed at $r_{DS} = \frac{1}{3}\sigma^{-1/2}$, where r_D is the Debye screening length in solution and $\sigma^{-1/2}$ is the separation between chains (Balastre, M.; Li, F.; Schorr, P.; Yang, J.; Mays, J. W.; Tirrell, M. V. *Macromolecules* **2002**, *35*, 9480−9486). The present experiments span this transition.

(71) Berggren, C.; Stalhandske, P.; Brundell, J.; Johansson, G. *Electroanalysis* **1999**, *11*, 156−160.

(72) Cai, W.; Peck, J. R.; van der Weide, D. W.; Hamers, R. J. *Biosens. Bioelectron.* **2004**, *19*, 1013−1019.

(73) Fritz, J.; Cooper, E. B.; Gaudet, S.; Sorger, P. K.; Manalis, S. R. *Proc. Natl. Acad. Sci. U.S.A.* **2002**, *99*, 14142−14146.

(74) Cloarec, J. P.; Deligianis, N.; Martin, J. R.; Lawrence, I.; Souteyrand, E.; Polychronakos, C.; Lawrence, M. F. *Biosens. Bioelectron.* **2002**, *17*, 405−412.

Supporting Information Available: Complete description of electrochemical and XPS experimental procedures, and derivation of eq 3. This material is available free of charge via the Internet at http://pubs.acs.org.

JA0571500